Thermo-spectral study of all-polymer multilayer lasers

James H. Andrews,[1] Michael Aviles,[1] Michael Crescimanno,[1] Nathan J. Dawson,[1] Anthony Mazzocco,[1] Joshua B. Petrus,[1] Kenneth D. Singer,[2,3] Eric Baer,[3] and Hyunmin Song[3]

[1]*Dept. of Physics & Astronomy, Youngstown State Univ., Youngstown, OH 44555, USA*
[2]*Dept. of Physics, Case Western Reserve Univ., Cleveland, OH 44106, USA*
[3]*Macromolecular Science and Engineering, Case Western Reserve Univ., Cleveland, OH 44106, USA*
jandrews@ysu.edu

Abstract: We investigate the temperature dependence of the emission wavelength and reflection band of polymer Distributed Bragg Reflector (DBR) and defect Distributed FeedBack (DFB) lasers fabricated using a coextrusion melt-process. We show the measured spectral shifts are a direct consequence of the optical path modifications associated with layer expansion and thermo-optic coefficients. By varying the choice of polymer bilayers and sandwiching the DBR laser films between glass coverslips, we fabricated DBR lasers that are either readily tunable up to 0.36 nm/°C or made thermally stable at 0.035 nm/°C.

OCIS codes: (140.3945) Microcavities; (160.5293) Photonic bandgap materials; (160.5470) Polymers; (160.6840) Thermo-optical materials; (230.1480) Bragg reflectors.

References and links

1. H. Song, K. D. Singer, J. Lott, Y. Wu, J. Zhou, J. H. Andrews, E. Baer, A. Hiltner, and C. Weder, "Continuous melt processing of all-polymer distributed feedback lasers," J. Mater. Chem. **19**, 7520–7524 (2009).
2. T. Kazmierczak, H. Song, A. Hiltner, and E. Baer, "Polymeric one-dimensional photonic crystals by continuous coextrusion," Macromol. Rapid Commun. **28**, 2010–2016 (2007).
3. H. Song, "Melt-processable polymeric photonic crystals and their applications as nano-layered laser films," Ph.D. thesis, Case Western Reserve University (2012).
4. G. Mao, J. Andrews, M. Crescimanno, K. D. Singer, E. Baer, A. Hiltner, H. Song, and B. Shakya, "Co-extruded mechanically tunable multilayer elastomer laser," Opt. Mater. Express **1**, 108–114 (2010).
5. J. H. Andrews, M. Crescimanno, N. J. Dawson, G. Mao, J. B. Petrus, K. D. Singer, E. Baer, and H. Song, "Folding flexible co-extruded all-polymer multilayer distributed feedback films to control lasing," Opt. Express **20**, 15580–15588 (2012).
6. K. D. Singer, T. Kazmierczak, J. Lott, H. Song, Y. Wu, J. Andrews, E. Baer, A. Hiltner, and C. Weder, "Melt-processed all-polymer distributed Bragg reflector laser," Opt. Express **16**, 10358–10363 (2008).
7. K. D. Singer, T. Kazmierczak, J. Lott, H. Song, Y. Wu, J. Andrews, E. Baer, A. Hiltner, and C. Weder, "Toward roll-to-roll production of polymer microresonator lasers," Opt. Photonics News **19**, 28–28 (2008).
8. J. Lott, H. Song, Y. Wu, J. Zhou, E. Baer, A. Hiltner, C. Weder, and K. D. Singer, "Coextruded multilayer all-polymer dye lasers," in *ACS Symposium Series: Organic Thin Films for Photonic Applications*, W. Herman, S. R. Flom, and S. H. Foulger, eds. (American Chemical Society, 2010), pp. 171–184.
9. J. Zhou, K. D. Singer, J. Lott, H. Song, Y. Wu, J. Andrews, E. Baer, A. Hiltner, and C. Weder, "All-polymer distributed feedback and distributed Bragg-reflector lasers produced by roll-to-roll layer-multiplying co-extrusion," Nonlinear Opt. Quant. Opt. **41**, 59–71 (2010).
10. N. Dawson, K. D. Singer, J. H. Andrews, M. Crescimanno, G. Mao, J. Petrus, H. Song, and E. Baer, "Post-process tunability of folded one-dimensional all-polymer photonic crystal microcavity lasers," Nonlin. Opt. Quant. Opt. **45**, 101–111 (2012).

#188683 - $15.00 USD Received 15 Apr 2013; accepted 10 Jul 2013; published 24 Jul 2013

11. D. M. Dattelbaum, S. A. Sheffield, D. Stahl, M. Weinberg, and C. Neel, "Equation of state and high pressure properties of a fluorinated terpolymer: THV 500," J. Appl. Phys. **104**, 113525 (2008).
12. J. F. Shackelford and W. Alexander, *Materials Science and Engineering Handbook*, 3rd ed. (CRC Press LLC, 2001).
13. J. M. Cariou, J. Dugas, L. Martin, and P. Michel, "Refractive-index variations with temperature of PMMA and polycarbonate," Appl. Opt. **25**, 334–336 (1986).
14. S. Krause and Z.-H. Lu, "Refractive index-temperature measurements on anionically polymerized polystyrene," J. Polym. Sci.: Polym. Phys. Ed. **19**, 1925–1928 (1981).
15. R. Simha and R. F. Boyer, "On a general relation involving the glass temperature and coefficients of expansion of polymers," J. Chem. Phys. **37**, 1003–1007 (1962).
16. S.-L. Chua, Y. Chong, A. D. Stone, M. Soljačić, and J. Bravo-Abad, "Low-threshold lasing action in photonic crystal slabs enabled by Fano resonances," Opt. Express **19**, 1539–1562 (2011).
17. M. Crescimanno, G. Mao, J. Andrews, K. Singer, E. Baer, A. Hiltner, H. Song, K. Comeau, B. Shakya, A. Bishop, and R. Livingston, "Role of group velocity delay in Faraday rotation in a multilayer polymer lattice," J. Opt. Soc. Am. B **29**, 1038–1047 (2012).
18. J. Yoon, W. Lee, J.-M. Caruge, M. Bawendi, E. L. Thomas, S. Kooi, and P. N. Prasad, "Defect-mode mirrorless lasing in dye-doped organic/inorganic hybrid one-dimensional photonic crystal," Appl. Phys. Lett. **88**, 091102 (2006).
19. E. Yablonovitch, "Inhibited spontaneous emission in solid-state physics and electronics," Phys. Rev. Lett. **58**, 2059–2062 (1987).
20. E. Yablonovitch, T. J. Gmitter, R. D. Meade, A. M. Rappe, K. D. Brommer, and J. D. Joannopoulos, "Donor and acceptor modes in photonic band structure," Phys. Rev. Lett. **67**, 3380–3383 (1991).
21. L. A. A. Pettersson, L. S. Roman, and O. Inganas, "Modeling photocurrent action spectra of photovoltaic devices based on organic thin films," J. Appl. Phys. **86**, 487–496 (1999).
22. Y. Wu, K. D. Singer, R. G. Petschek, H. Song, E. Baer, and A. Hiltner, "Mode delocalization in 1D photonic crystal lasers," Opt. Express **17**, 18038–18043 (2009).

1. Introduction

Previous work [1–3] has demonstrated that all-polymer coextruded microcavity lasers can be be fabricated from a variety of polymers and dyes and in many tailorable layerings, resulting in broad mechanical and structural tunability [4, 5]. We report here on a study of the temperature dependence of the laser emission wavelength and its relation to thermally-induced changes in the underlying structure's reflection band features. Two types of all-polymer lasers are studied as a function of temperature; (1) Distributed FeedBack (DFB) lasers that are made of alternating layers of undoped and dye-doped polymers and folded to create a defect DFB laser [5], and (2) Distributed Bragg Reflector (DBR) lasers that use a thick dye-doped polymer as the active gain medium between the cavity reflectors consisting of bilayers of refractive-index mismatched polymers [6–9]. Both laser types use multilayers of alternating, refractive index mismatched polymers to produce a reflection band. Roughly, the reflection band's center wavelength depends on average layer (optical) thickness and the band's spectral width depends on the difference in refractive index between the two materials, and the number of bilayers. Both the layer thicknesses and the refractive indices are, to differing extents, temperature dependent.

The microcavity lasers in this research used rhodamine 6g (R6G) dopant as the gain element in the host polymers. These R6G lasers have previously been shown to operate at a range of wavelengths between 555-650nm for the defect DFB lasers [10] and 565-615nm for the elastomer DBR lasers [4]. From this large range of available lasing wavelengths, the particular lasing wavelength has been shown in the cited work above to be controllable through deliberate structural design and materials selection. We report here on the measured temperature tunability and stability of these microcavity lasers. A simple, quantitative, linear optical model captures many features of the temperature tunability in these multi-layered microcavity lasers, indicating promise for a more targeted co-extruded polymer laser development and improved understanding of thermo-spectral effects in polymer multilayers generally.

#188683 - $15.00 USD Received 15 Apr 2013; accepted 10 Jul 2013; published 24 Jul 2013

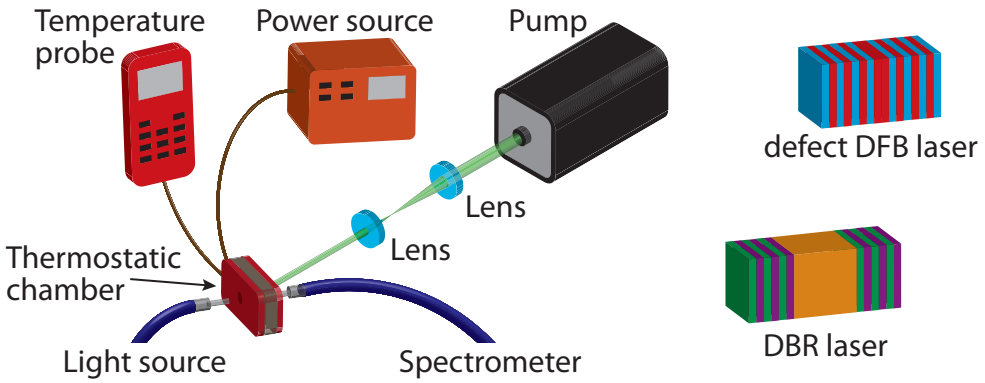

Fig. 1. An adjustable thermostatic chamber surrounds the film sample holder while allowing optical access for the transmittance and laser emission spectra measurements. Diagrams of the multilayer schema for the defect DFB and DBR lasers are shown to the right of the experiment schematic.

2. Materials and multilayer film experiments

The DFB lasers are fabricated by a melt-process co-extrusion technique producing 32 bilayers (64 layers) in the initial extruded films, which are then folded to create a defect DFB laser [5]. Each bilayer is comprised of a fluoroelastomer terpolymer layer of vinylidene fluoride, hexafluoropropylene, and tetrafluoroethylene (Dyneon THV 220G, refractive index=1.37) and an R6G dye-doped blended polymer layer of 75 wt% polystyrene and 25 wt% acrylonitrile (SAN25, refractive index=1.57) [1]. The bilayers have an average periodicity of 200 nm with an $\sim$ 18% layer-to-layer thickness variation, and with a 1% nominal concentration of R6G in the SAN25 layer [2, 9]. Here, we separately test films folded in each direction, to produce either a doubled THV or doubled SAN25 center layer.

The DBR lasers are also fabricated by melt-process co-extrusion, but with 64 bilayers (128 layers) laminated above and below a single center gain layer consisting of an ethylene terpolymer composed of 40 wt% acrylic ester and glycidyl methacrylate (Lotador 8900) doped with 1 wt% R6G, and with a thickness of $\sim 15\,\mu$m (before folding). For one type of DBR laser, each bilayer is comprised of a layer of ethylene-octene (EO) (Dow Engage 8842, refractive index=1.48) and a layer of THV. These were co-extruded with the doped Lotador skin layer over which the multilayer EO/THV films were folded to create an elastomer DBR laser, i.e., a 30 μm active medium sandwiched between two 128-layer elastomeric multilayer reflectors [4]. The other DBR laser type is made by first stacking four 32-layer films made of alternating layers of polystyrene (PS, refractive index=1.59) and poly(methyl methacrylate) (PMMA, refractive index=1.49) [6]. These stacked films are laminated on each side of a stand-alone dye-doped Lotador layer to create a $\sim 30\,\mu$m R6G-doped Lotador gain layer sandwiched between two 128-layer polymer multilayer reflectors. In both DBR laser types, the bilayers have an average periodicity of $\sim$ 220 nm with a $\sim$ 25% layer-to-layer thickness variation. For both DBR laser types, the constructed laser films were then sandwiched between glass coverslips which had been prepared so that the films adhered to the glass surface without slipping (hereafter referred to as 'pinned' DBR lasers).

The multilayer laser films are then placed in an insulated adjustable thermostatic chamber as shown in Figure 1 with optical windows to transmit pump and probe beams and a broadband source used for measuring the films' transmission spectra. All laser films are pumped by a 7 ns pulsed 532 nm coherent laser source from a frequency-doubled YAG laser, which coincides

#188683 - $15.00 USD Received 15 Apr 2013; accepted 10 Jul 2013; published 24 Jul 2013

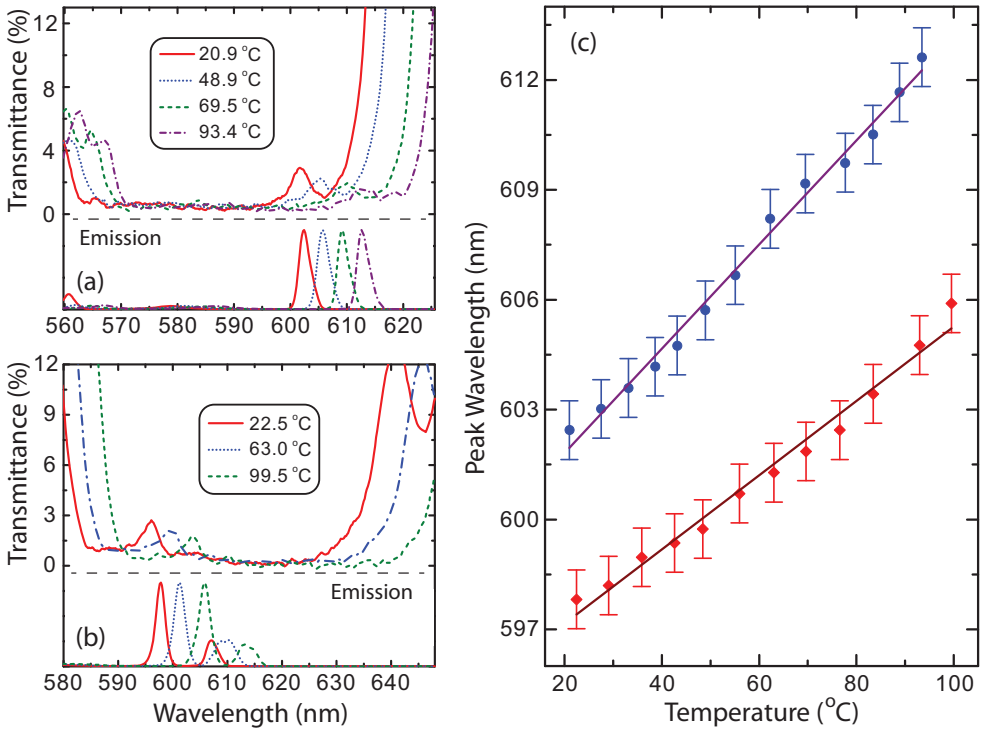

Fig. 2. The transmission and emission spectra of defect DFB laser films folded on (a) THV and (b) SAN25 at different temperatures. (c) The peak lasing wavelength as a function of temperature for defect DFB lasers folded on (blue circles) THV and (red diamonds) SAN25. The solid lines are linear fits to the experimental data.

with the absorption band of R6G. An Ocean Optics USB 4000 spectrometer records the lasing wavelength(s) of the multilayer laser films and the transmission spectrum of the multilayer films at different temperatures.

3. Results and modeling parameters

3.1. Defect DFB lasers

Figure 2 shows sample reflection and emission spectra from a defect DFB laser folded onto (a) the THV side and (b) the SAN25 side, respectively. The corresponding temperature shifts of the peak lasing wavelength are shown in Fig. 2(c). The emission wavelength, λ_e, at room temperature and the peak laser wavelength's temperature coefficient, $(1/\lambda_e)\, d\lambda_e/dT$, ($T$ is the temperature) are given in Table 1.

We note that when the reflection band defect is near the short wavelength bandedge (as seen for the sample folded on the SAN25 center layer), the lasing wavelength's temperature coefficient is noticably smaller than when the reflection band defect is nearer the long wavelength bandedge (as for the sample folded on the THV side). As further discussed below, the initial defect locations imply that the optical thickness of the center SAN25 layer is less than the average optical thickness of the constituent bilayers, whereas the optical thickness of the center THV layer is greater than the average optical thickness of the constituent bilayers [5].

#188683 - $15.00 USD Received 15 Apr 2013; accepted 10 Jul 2013; published 24 Jul 2013

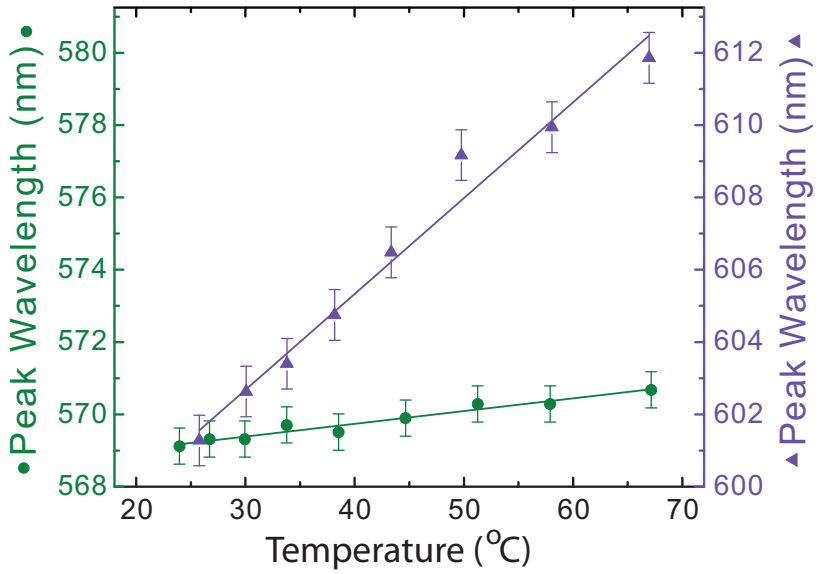

Fig. 3. The peak lasing wavelength as a function of temperature for two DBR lasers made by laminating an R6G-doped Lotador cavity between 128-layer films of alternating THV/EO (right, blue triangles) and PS/PMMA (left, green circles). The lines in both graphs are the linear fits the experimental data. Note that the right and left axes are drawn to the same scale but over slightly shifted spectral regions.

3.2. DBR lasers

The first DBR laser studied is that of a $\sim 30\,\mu$m layer of Lotador confined between two 128-layer reflectors made from alternating layers of THV and EO, all of which are elastomeric, as previously described, but then placed between rigid glass coverslips. The peak lasing wavelength is plotted with respect to temperature in Fig. 3(left axis). The second DBR laser, a $\sim 30\,\mu$m dye-doped Lotador gain medium between 128-layer PS/PMMA reflectors, also between glass coverslips, resulted in the plot of peak lasing wavelength as a function of temperature shown in Fig. 3 (right axis). The emission wavelength and wavelength temperature coefficient for both pinned DBR laser types are given in Table 1.

3.3. Thermo-optic and thermal strain characterization

The thermo-optic coefficients and thermal strain coefficients used to model the laser wavelength temperature dependence are given in Table 2. The thermo-optic coefficients, i.e., the temperature dependence of the refractive indices, for most of the constituent polymers were

Table 1. Thermo-spectral emission shifts ($\times 10^{-4}/^{\circ}$C)

Laser type	Center material	Reflector material	$(1/\lambda_e)\,d\lambda_e/dT$
Defect DFB	THV	THV/SAN25	2.33 ± 0.17
Defect DFB	SAN25	THV/SAN25	1.68 ± 0.17
Pinned DBR	Lotador	THV/EO	6.00 ± 0.50
Pinned DBR	Lotador	PS/PMMA	0.61 ± 0.29

#188683 - $15.00 USD Received 15 Apr 2013; accepted 10 Jul 2013; published 24 Jul 2013

Table 2. Thickness (L) and Refractive Index (n) Temperature Dependence ($\times 10^{-4}/^{\circ}$C)

Material	$(1/L)dL/dT$	dn/dT
THV	$2.14 \pm 0.08^{\S\flat}$	$-2.63 \pm 0.24^{\ddagger\flat}$
SAN25	$0.66 \pm 0.01^{\dagger}$	$-1.28 \pm 0.26^{\ddagger\flat}$
PMMA	$0.65^{\diamond}$	$-1.40 \pm 0.1^{\ddagger\sharp}$
PS	$0.73 \pm 0.13^{\P\dagger}$	$-1.4 \pm 0.1^{\natural}$
EO	$5.1 \pm 2.0^{\P}$	$-3.6 \pm 0.5^{\ddagger}$
glass substrate	< 0.1	

‡ Ellipsometry § Interferometry ♭ Defect spectrum fits
¶ Grating method † Ref. [12] ♯ Ref. [13]
♮ Ref. [14] ⋄ Ref. [15]

first measured using a Horiba Uvisel DUV-NIR spectroscopic ellipsometer for which the initial fits were refined through fits to the spectral data. Where possible, these values are also compared with values found in the literature. To perform these measurements, thin monoliths were spin-coated on silicon wafers and the measurements were performed with a probe beam at 70° from the direction normal to the substrate. Slow temperature drifts and calibration issues as well as difficulties in the optimization of multi-parameter refractive models are the leading contributions to the uncertainties.

The linear thermal expansion coefficients were measured for monoliths of most of the constituent materials. In addition to measuring the thickness changes directly through temperature dependent profilometery, we also measured thermal expansion coefficients using Fabry Perot interferometry or by diffraction from embossed gratings on the surfaces of the films. For example, the thermal expansion coefficient of THV (and other monoliths) was measured by pinning two 'pillars' $< 50\mu m$ high of the monolith films as thermally tunable spacers between mirrored surfaces forming an air-gapped Fabry-Perot interferometer. Using a 632.8 nm HeNe laser, we monitored the fringes during heating to determine the thermal expansion of the pillars. Note that these pillars were thin enough and affixed well enough that their expansion parallel to the mirrored surfaces was mechanically pinned. Because the mirrored surfaces were gold sputtered on glass, which had a comparatively negligible thermal expansion, the measured thermal expansion in the cavity length was effectively a measure of the volumetric thermal expansion of the polymers. Additionally, the cavity was only lightly mechanically loaded for geometrical rigidity. Because THV loses stiffness when heated, the applied compressional force on the cavity may reduce the overall expansivity of THV [11], indicating that this technique may underreport the volumetric thermal expansivity.

4. Modeling and Discussion

The physical parameters contributing to any laser's wavelength temperature dependence are its gain envelope shift and the combined effects of thermal strain and index change of the passive optical components that comprise the laser cavity. In multilayer laser films with a broad gain envelope the "optical geometry" (i.e., the list of layer optical thicknesses) is typically the dominant effect that selects the laser's wavelength. Indeed, wavelength tunings via stretching and terracing the DFB and DBR lasers of Refs. [4, 5] make the case for the significance of structure as compared to shifts in the gain envelope abundantly clear for the lasers studied in this report

#188683 - $15.00 USD Received 15 Apr 2013; accepted 10 Jul 2013; published 24 Jul 2013

(compare with Chua, *et al.* [16]). This dependence on structure in turn implies that simple linear optical models based with the thermal expansitivities and thermo-optic coefficients of their constituent layers should both qualitatively and quantitatively capture the relevant phenomena reported above.

Below we test this assertion using as inputs only the gross structural morphology of each of the laser types studied here and the measured thermal and optical properties of the constituent polymers as detailed in Table 2. Note, however, that in our modeling, we have modified the starting thermal expansion coefficients given in Table 2 in the DFB films to account for the relative pinning of the softer of the two polymers by constraining its expansion in the plane to the expansion of the other polymer and, in the case of the DBR lasers, to account for the pinning of the multilayer polymer films to the much less thermally expansive glass coverslips. Thus, we assumed that the THV layers in the DFB laser films were constrained to expand in the plane only as much as the more rigid SAN25 layers, leading to a nearly three times greater thermal expansivity for the THV layer thicknesses. Similarly, all of the DBR films were constrained by the glass coverslips to not expand appreciably in the plane, leading to enhanced thermal expansion of the thickness of the films. We saw no evidence of delamination of the films during any of our experiments.

First, qualitatively and in gross effect, thermal expansion causes the spectral features of the multilayer interference to shift toward longer wavelengths. However, each constituent polymer listed in Table 2 has a negative thermo-optic coefficient, which, taken by itself, would shift the spectral features to shorter wavelengths. With both effects taken concurrently for these materials, experiment and linear transport models using the inputs from Table 2 indicate that thermal expansion typically dominates the index changes for our materials and thus the optical path length (and bands and band features) shifts to longer wavelength with increasing temperature.

Both experiment and linear transport modeling, however, indicate that this redshift with temperature is not uniform across the reflection band, but is greater near the long wavelength band edge. To model this effect, we first assume perfect layer thicknesses except for the center layer, which is adjusted to a thickness that creates a band defect at the desired location near the right or left edge of the reflection band. We used a least squares fitting routine to obtain theoretical parameters (thermal expansion and thermo-optic coefficients) by fitting the calculated shifts in spectral features (band edge and defect shifts) from transfer matrix methods to those obtained via experiments. We used values obtained from ellipsometry and interferometry measurements as the initial parameters. To get a unique fit, we held the thermal expansion coefficient of SAN25 (given in Ref. [12]) constant and optimized the relative thermal shifts using the other three parameters (thermal expansion and thermo-optic coefficients of THV and thermo-optic coefficient of SAN25) . The fitting values, listed in Table 2, are in good agreement with the literature and independent monolith measurements. In these binary films, optical transport near the short wavelength band edge corresponds to the light spending more time in the high index material (which here has a smaller temperature coefficient) and vice-versa at the long wavelength band edge where transport is dominated by the wave's presence in the low index material (which here has a higher temperature coefficient) [17]. Our modeling bears out this relationship as well, indicating that, for these materials, the ratio of the thermo-spectral band edge shifts is predicted to be 1.6 ($\pm$.1), very close to our experimentally measured ratio for the band edges. (The measured short wavelength band edge shifts as $(1/\lambda)(d\lambda/dT) = (1.51 \pm .16) \times 10^{-4}/^{\circ}\mathrm{C}$, and the measured long wavelength band edge shifts as $(1/\lambda)(d\lambda/dT) = (2.35 \pm .25) \times 10^{-4}/^{\circ}\mathrm{C}$.)

The defect DFB lasers exhibit low-threshold, coherent emission at the reflection band defect's spectral location [5,18]. Therefore, simply recording the shift in the reflection band defect in simulations with linear coefficients as a function of temperature yields the defect DFB laser's temperature coefficient. The defect's position in the reflection band is a function of the optical

#188683 - $15.00 USD Received 15 Apr 2013; accepted 10 Jul 2013; published 24 Jul 2013

phase accumulated in the central layer [19, 20]. Thus, each defect DFB laser's wavelength temperature coefficient depends on the temperature shift of the reflection band, the initial spectral location of the defect within that band, and the properties of the material used for the center defect layer.

Calculations of the energy density during steady state linear transport in these defect DFB's indicate that the light spends more time in the centermost region of the film [21]. In keeping with the description above, as one adds thickness (and thus phase accumulation) to the center layer, the resulting band defect initially moves towards longer wavelength as the portion of the time it spends in the lower index material increases. Quantitatively, linear transfer matrix modeling confirms that each defect DFB laser's temperature coefficient is strongly dependent on where in the reflection band the defect occurs [5]. This result is relevant because our experiments show that spectral defects from THV-folded systems appear near the long-wavelength edge of the reflection band, whereas the defects from SAN25-folded systems are closer to the short-wavelength edge of the reflection, artifacts of layer thickness deviations in our films embedded during the co-extrusion process [10].

Numerical simulations of the location of the defect relative to the band edges show that the ratio of the temperature coefficients $(1/\lambda)(d\lambda/dT)$ from the long wavelength band edge over the short wavelength band edge can be as high as 1.7 ($\pm$.1). This ratio is consistent with the results shown in Table 1 and with the locations of the individual band edges for our THV and SAN25 centered films. Further, in as much as there is a difference between this ratio and that of the individual band edges, it may be simply understood in terms of the 'persistence' of the light in the center element of the stack for the defect mode (as indicated by the energy density calculations) compared with the nearly evanescent state at the band edges, which do not preferentially sample the center layer.

The DBR data (Fig. 3) qualitatively reinforces these lessons. While the complexities in this case (whose central gain layer, at $\sim$ 30 microns, is significantly wider than the mirrors, each about 7 microns) make a quantitative theoretical model of the laser wavelength temperature coefficient more daunting, the difference between the two DBR cases in Fig. 3 provides evidence that it is the DBR mirror temperature coefficient and not the central layer's expansion that dominates the laser's temperature coefficient.

Analytical models as simple as a linear optical three layer dielectric (with gain in the middle element and thin, large index 'mirrors' on each end) also emphasize the role that the mirrors' transmission features have on the density of states, thereby both increasing the gain and reducing the cavity mode spacing. Thus, although the penetration into the mirrors is only about 4 microns [22] and cannot account, by itself, for the data in Fig. 3, it is the tight association of the transmission features of the mirrors with lasing that force the DBR lasers' temperature coefficients to follow those of the DBR mirrors alone. This result is consistent with the conclusion from Ref. [4], where the DBR lasing wavelength was closely tied to that of transmission defects.

5. Conclusions

The temperature tunability and stability of all-polymer DBR and defect DFB laser films have been studied for select materials. We found that for DBR laser films, the temperature dependence of the laser wavelength was dominated by the mirrors and not the (much larger) gain medium. Thus, cavities with PS/PMMA (low temperature coefficient) reflectors make DBR lasers that are temperature stable. The output wavelength of DBR lasers with the very same gain element but with EO/THV reflectors (two elastomers with large thermal expansions) have a large temperature coefficient, indicating a $>$10 nm tuning range across a 30° temperature shift. Similarly, defect DFB laser's thermal coefficients are found to depend mainly on the location

#188683 - $15.00 USD Received 15 Apr 2013; accepted 10 Jul 2013; published 24 Jul 2013

of the reflection band defect and the relative index of refraction of the center layer.

Significantly, a simple optical transport model based on transfer matricies quantitatively reproduces the observed defect DFB laser behavior, and qualitatively illuminates the DBR laser temperature dependence. In both cases, experiments and simulations indicate that the temperature coefficients of the multilayer mirrors are paramount in determining the temperature coefficient of the lasing wavelength. This work confirms that other factors that one might have expected to have contributed to the temperature coefficient, such as gain envelope temperature dependence, thermal strain of the centermost fold layer (defect DFB) and thermal strain of the gain medium (DBR) are less important.

Acknowledgments

The authors are grateful to the National Science Foundation for financial support from the Science and Technology Center for Layered Polymeric Systems under grant number No. DMR 0423914 and to the State of Ohio, Department of Development, State of Ohio, Chancellor of the Board of Regents and Third Frontier Commission, which provided funding in support of the Research Cluster on Surfaces in Advanced Materials.

#188683 - $15.00 USD Received 15 Apr 2013; accepted 10 Jul 2013; published 24 Jul 2013